Critical Magnetic Scattering in K_2NiF_4 †

R. J. Birgeneau
Bell Laboratories, Murray Hill, New Jersey 07974

and

Brookhaven National Laboratory, Upton, New York 11973
and
J. Skalyo, Jr. and G. Shirane
Brookhaven National Laboratory, Upton, New York 11973
(Received 16 October 1970)

A detailed study of the static and dynamic critical behavior of the planar antiferromagnet K_2NiF_4 is reported. The dynamic experiments reveal several unusual features. Magnons over most of the Brillouin zone are observed to persist well above T_N. The magnons ultimately become unobservable because of lifetime effects rather than any appreciable renormalization of the real part of the energy. The spin-wave gap remains sharp right up to the phase transition and, in fact, it seems to renormalize like the sublattice magnetization at all temperatures. The transverse excitations for $q \neq 0$ in general exhibit no explicit recognition of the phase transition and even at $q = 0$ there is no apparent variation through T_N of the integrated intensity. The function $S^{\parallel}(\vec{q}, \omega)$, which manifests the expected critical behavior, is found to be very narrow in q, ω space. For $T < T_N$ there is no measurable inelasticity of the critical fluctuations at $q = 0$. For $T > T_N$, $S^{\parallel}(0, \omega)$ has a finite width which goes to zero as $T \to T_N^+$ thus exhibiting the critical slowing down first predicted by Van Hove. Quasielastic measurements of $\chi^{\parallel}(\vec{q})$ have been carried out for $T \geq T_N$. These experiments yield the critical exponents $\eta = 0.4 \pm 0.1$ measured at T_N and $\nu = 0.57 \pm 0.05$, $\gamma = 1.0 \pm 0.1$ for $T > T_N$. The value for η is similar to that for the two-dimensional Ising model, $\eta = 0.25$, but ν, γ differ considerably from the Ising-model values of $1, \frac{7}{4}$. This latter result is not in agreement with current theory.

I. INTRODUCTION

In several recent papers we have reported neutron-scattering investigations of various aspects of the static and dynamic properties of the planar antiferromagnet K_2NiF_4.[1-3] The principal result of these studies is that K_2NiF_4 has a pronounced two-dimensional ([2]) character and, in particular, it seems to exhibit what may be described as a genuine [2] second-order magnetic phase transition. In the static experiments, which measure the Fourier transform of the equal-time pair-correlation function, it is found that in the paramagnetic regime the critical scattering has the form of *ridges* rather than *peaks*; these ridges, which extend in the direction perpendicular to the NiF_2 planes, are found to be absolutely independent of that momentum coordinate, thus showing that the correlations are entirely two dimensional. As the temperature is lowered towards the ordering temperature, the scattering intensity at the superlattice position grows and the ridge narrows, corresponding to continuous increases in the staggered susceptibility and the correlation length, respectively. At 97.23 °K, the system undergoes a magnetic phase transition; however the actual transition is three dimensional, that is, the system achieves long-range order simultaneously both within the NiF_2 planes and between them. The crucial feature is that the ordering is not accompanied by any observable [3] critical scattering both above and below T_N. This immediately leads one to conclude that the phase transition is driven by the planes themselves and that the [3] aspects are inessential.[4] From a study of the geometry of the critical scattering, it is also found that only $\chi^{zz}(0)$, the component of the [2] staggered susceptibility along the anisotropy direction, diverges at T_N.[3] It therefore seems that the anisotropy is playing an important role. In fact, it is probably this anisotropy which enables the [2] NiF_2 planes to order, since a [2] Heisenberg system cannot exhibit conventional long-range order for $T > 0$.[5]

To date, studies of the dynamics of K_2NiF_4 have been limited to a measurement of the spin-wave dispersion relations at 5 °K and an initial investigation of the long-wavelength magnons around T_N.[2] The low-temperature measurements showed that magnons propagating within the planes are accurately described by simple spin-wave theory with a nearest-neighbor Heisenberg exchange $J = 9.68 \pm 0.06$ meV ($\mathcal{H} = J\vec{S}_1 \cdot \vec{S}_2$) and an anisotropy field $g\mu_B H_A = 0.073 \pm 0.001$ meV. The spin-wave energies were also found to be independent of the momentum component perpendicular to the NiF_2 planes to within an experimental accuracy of 1 part in 270. Several long-wavelength magnons, and in particular one at

$E = 7$ meV with $\vec{q} \sim 0.05$ reciprocal-lattice units (i.e., $\lambda \simeq 110$ Å) were followed through T_N. Somewhat surprisingly, it was found that the 7-meV magnon changed little in either energy or width up to $\sim 1.1 T_N$.

So far, studies of the critical exponents have been limited to a measurement of the sublattice magnetization which yields $\beta = 0.138 \pm 0.004$; this is extremely close to the value $\beta = 0.125$ appropriate to the [2] $S = \frac{1}{2}$ Ising model. Recent numerical work[6] has indicated that the critical exponents in the asymptotic limit should depend only on the symmetry of the Hamiltonian and not on its details. This fact, together with the observed value for β, would seem to suggest that K_2NiF_4 might indeed exhibit critical behavior similar to that predicted for the [2] Ising model.

In this paper, we report detailed studies of the static and dynamic critical behavior of K_2NiF_4 employing precise resolution corrections. It was originally hoped that it would prove possible to study the critical dynamics with sufficient accuracy to be able to test the dynamic scaling ideas of Farrell *et al.* and Halperin and Hohenberg in two dimensions.[7-9] However, both because of the narrowness of the critical mode in q, ω space and simple signal-to-noise problems we have been limited to a semiquantitative survey of the dynamics around T_N. For the statics, however, because one integrates over energy there is no signal-to-noise problem and we are able to measure the static critical exponents accurately. In this paper we report measurements of $\chi^+(0)$, the staggered susceptibility for $T > T_N$, κ^+ the inverse correlation length for $T > T_N$, and $\chi(\vec{q})$ at T_N. Measurements for $T < T_N$ will be reported at a later date.

The format of the paper is as follows. In Sec. II, we review the general theory of magnetic neutron scattering, particularly as applied to two-dimensional systems. We discuss in detail the theory for the static measurements where we show that there is an important simplification in obtaining $\int d\omega$ in one- and two-dimensional systems. In Sec. III, the details of the experimental technique and the methods of data analysis are presented. The experimental results for the dynamics are described in Sec. IV, while the static critical behavior measurements are presented in Sec. V.

II. THEORY

A. Neutron Scattering

The magnetic neutron-scattering cross section for unpolarized neutrons from N localized spins is[10]

$$\frac{\partial^2\sigma}{\partial\Omega_f \partial E_f} = A(\vec{k}_i, \vec{k}_f) \sum_{\alpha\beta} (\delta_{\alpha\beta} - \hat{Q}_\alpha \hat{Q}_\beta) S^{\alpha\beta}(\vec{Q}, \omega), \qquad (1)$$

where the momentum transfer $\hbar\vec{Q} = \hbar\vec{k}_i - \hbar\vec{k}_f$, the energy transfer

$$\hbar\omega = (\hbar^2/2m_0)(k_i^2 - k_f^2),$$

and $A(k_i, k_f)$ is a constant depending on the moment, the form factor, and k_i, k_j, Here

$$S^{\alpha\beta}(\vec{Q}, \omega) = (1/2\pi) \int_{-\infty}^{\infty} e^{i(\vec{Q}\cdot\vec{r} - \omega t)} \sum_{\vec{r}} \langle S_0^\alpha(0) S_{\vec{r}}^\beta(t) \rangle \, dt \ , \qquad (2)$$

that is, the scattering cross section is directly proportional to the space-time Fourier transform of the unequal-time two-spin correlation function. For systems with Heisenberg interactions and uniaxial anisotropy, only the diagonal components $\alpha = \beta$ are nonvanishing. The component of $S^{\alpha\beta}(\vec{Q}, \omega)$ associated with the fluctuations may be written

$$S_D^{\alpha\beta}(\vec{Q}, \omega) = (k_B T/g^2\mu^2)\chi^{\alpha\beta}(Q) \times (\hbar\omega\beta/1 - e^{-\hbar\omega\beta}) F^{\alpha\beta}(\vec{Q}, \omega), \qquad (3)$$

where the frequency distribution function $F^{\alpha\beta}(\vec{Q}, \omega)$ has the property that

$$\int d\omega \, F^{\alpha\beta}(Q, \omega) = 1 . \qquad (4)$$

$\chi^{\alpha\beta}(\vec{Q})$ is the wave-vector–dependent susceptibility. Equation (5) is simply a statement of the well-known fluctuation-dissipation theorem.[11]

In the dynamics experiments one is interested in detailed studies of $F^{\alpha\beta}(\vec{Q}, \omega)$. If, for instance, one assumes that the correlations decay exponentially in time, then $F^{\alpha\beta}(\vec{Q}, \omega)$ will have the form of a simple Lorentzian in the energy

$$F^{\alpha\beta}(\vec{Q}, \omega) = \pi^{-1}[\Gamma(\vec{Q})/\omega^2 + \Gamma(\vec{Q})^2]. \qquad (5)$$

If, in addition, the correlations have an oscillation in time with frequency $\omega(\vec{Q})$ superimposed on the exponential decay, then (5) becomes two displaced Lorentzians centered about $\pm\omega(\vec{Q})$.

For the longitudinal component near T_N, one expects $F^{zz}(\vec{Q}, \omega)$ to have a Lorentzian frequency spectrum as in (5). The transverse components in an anisotropic system however may well have a magnonlike shape near T_N, approximating closely displaced Lorentzians. Indeed we have already observed experimentally that long-wavelength magnons persist up to $1.1\ T_N$.

Using (4), Eq. (3) may be rewritten

$$\int_{-\infty}^{\infty} d\omega \left(\frac{1 - e^{-\hbar\omega\beta}}{\hbar\omega\beta}\right) S_D^{\alpha\beta}(\vec{Q}, \omega) = \frac{k_B T}{g^2\mu^2} \chi^{\alpha\beta}(\vec{Q}) . \qquad (6)$$

For the critical fluctuations under normal conditions the major contributions to $\chi^{\alpha\beta}(Q)$ come in the region $\hbar\omega \ll k_B T$. In that case,

$$(1 - e^{-\hbar\omega\beta}/\hbar\omega\beta) \simeq 1,$$

so that (6) becomes

$$\int_{-\infty}^{\infty} d\omega \, S_D^{\alpha\beta}(Q, \omega) = (k_B T/g^2\mu^2)\chi^{\alpha\beta}(\vec{Q}) ; \qquad (7)$$

hence by measuring $\int_{-\infty}^{\infty} d\omega\, S^{\alpha\beta}_D(Q,\omega)$, we may in fact measure directly the wave-vector-dependent susceptibility. In Sec. IIC, we discuss the problems in obtaining $\int d\omega$ experimentally.

B. Wave-Vector-Dependent Susceptibility

The wave-vector-dependent susceptibility has been discussed in detail for the [2] and [3] Ising models by Fisher and Burford.[12] They show that to rather high accuracy for $T \geq T_c$ one may write

$$\chi(\vec{q})/\chi_0 = (1/r_1)^{2-\eta}(\kappa^2+\varphi^2 q^2)^{\eta/2}/(\kappa^2+\psi q^2)\,, \qquad (8)$$

where, in two dimensions, $\eta = \frac{1}{4}$ and $\varphi(T)$ is a slowly varying function with magnitude 0.03 at T_c; $\psi = 1 + \frac{1}{2}\eta\varphi^2$ which is very close to 1. χ_0 is the Curie susceptibility for noninteracting spins. For $T = T_c$, Eq. (8) becomes

$$\chi(\vec{q})/\chi_0 = (1/r_1)^{2-\eta}(\varphi^\eta/q^{2-\eta})\,, \qquad (9)$$

whereas for $T > T_c$ and $q < \kappa/\varphi$

$$\chi(\vec{q})/\chi_0 \simeq (1/r_1)^{2-\eta}(\kappa^\eta/\kappa^2+q^2)\,. \qquad (10)$$

These two forms are consistent with the exact results of Kaufman and Onsager[13] and Kadanoff and Wu[14] for the [2] Ising model. In the past various workers have tended to use Eq. (8) either with $\eta = 0$, the classical Ornstein-Zernike form, or with $\varphi = 1$, $\psi = 1$ which is known as Fisher and Burford's "first approximant." In [3] systems where η is small, the final results tend to be insensitive to the explicit form used. However, as we shall see, in two dimensions η may be quite large and in that case the specific analytic form chosen for $\chi(\vec{q})$ is quite important. Finally, in K_2NiF_4 we have the additional complication that there is no explicit theory for a [2] near-Heisenberg antiferromagnet. We must therefore use Eqs. (8)–(10) only as a guide with the final form being dictated by the experimental results themselves.

C. Quasielastic Approximation

From Eq. (7) we see that the wave-vector-dependent susceptibility is proportional to $\int d\omega\, S_D(\vec{Q},\omega)$ provided only that $\hbar\omega \ll k_B T$. Thus we may in theory obtain $\chi^{\alpha\beta}(\vec{Q})$ by measuring $S_D(\vec{Q},\omega)$ directly and integrating over ω. In practice, however, this is not possible in most cases. The usual experimental technique is instead to remove the ω discrimination and simply to accept all neutrons emerging at a given scattering angle. This yields $\int dk_f A(k_i,k_f) S_D(\vec{Q},\omega)$, which is proportional to $\int d\omega\, S_D(\vec{Q},\omega)$ provided that the reduced parameter

$$[(m_0/\hbar)\Gamma/k_i\kappa] \ll 1\,, \qquad (11)$$

where Γ is an average characteristic frequency, k_i is the incident neutron wave vector, and κ is the inverse correlation length. This simply requires that the change in k_f involved in integrating over ω be small compared with κ, or in more physical terms, that the neutron pass through a region of correlated spins in a time fast compared with the fluctuation period.

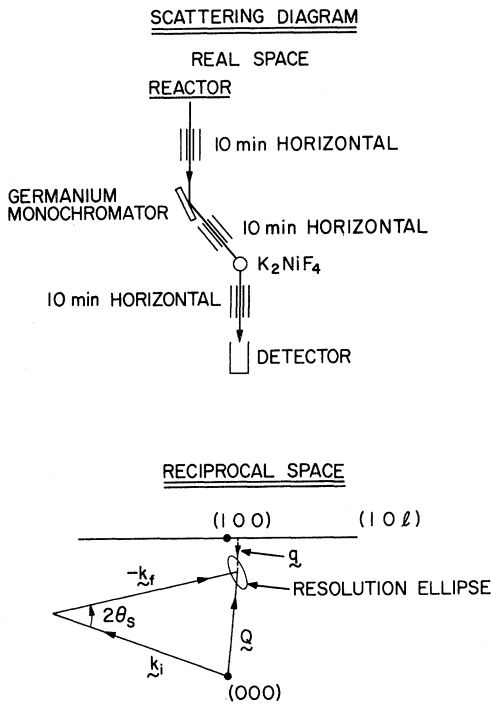

FIG. 1. Diagram of a two-axis neutron spectrometer. Lower portion gives the equivalent scattering in reciprocal space.

In one- and two-dimensional systems, however, an important simplification occurs which enables us to measure $\int d\omega$ directly. This is best described by explicitly considering the scattering diagram. In Fig. 1, we show a typical experiment setup in a two-axis experiment. The corresponding scattering diagram in reciprocal space is shown in the bottom part of the figure. In a [3] experiment, the reduced-momentum vector would be measured from the (1, 0, 0) reciprocal-lattice vector. As discussed by Schulhof *et al.* (Ref. 15) this immediately leads one to condition (11). In two dimensions, however, if (0, 0, l) is the direction perpendicular to the magnetic planes, then q is measured from the closest point along (1, 0, l) rather than (1, 0, 0). It is trivial to show that (11) then becomes

$$[(m_0/\hbar)\Gamma/k_i\kappa]\sin\theta_f \ll 1\,, \qquad (12)$$

where θ_f is the angle k_f makes with the (1, 0, l) ridge. Condition (12) may always be satisfied by choosing the scattering geometry such that $\theta_f = 0$, that is, by having k_f parallel to the ridge. In this case, changing k_f does not change the momentum transfer within the planes, so that the integration over the energy is performed properly. If we

choose local axes such that z is along the ridge and x is perpendicular to it, then for $Q \ll k_i$, $\theta_j = 0$ when

$$Q_z = Q_x \frac{Q_x/2k_i}{[1-2(Q_x/2k_i)^2]^{1/2}} . \quad (13)$$

In order to illustrate the effects of inelasticity for various geometries we have carried out a computer simulation of a constant-angle experiment. The results of this study for several values of the reduced parameter $(m_0\Gamma/\hbar)/k_i\kappa$ are shown in Fig. 2. This was calculated for the experimental setup shown in Fig. 1 with the x and z axes defined as above, $Q_x = 1$, $k_i = 6$, and Γ taken at a constant value independent of q. It assumes

$$S^{zz}_D(q,\omega) \propto \frac{1}{\kappa^2+q^2}\frac{1}{\pi}\frac{\Gamma}{\Gamma^2+\omega^2} , \quad (14)$$

and the xx, yy components are neglected for purposes of this illustration. From the figure it may be seen that the inelasticity may indeed have significant effects on each of $\chi(0)$ and κ. However, both are properly determined when (12) is satisfied.

In a one-dimensional system the requirement for $\theta_f = 0$ is simply that $\vec{k}_f$ must be perpendicular to the chains.

III. EXPERIMENTAL TECHNIQUE

A. Sample and Apparatus

The crystal structure of K_2NiF_4 and, in particular, the structural reasons for the [2] behavior, have been discussed at some length previously.[1-3] A diagram of the structure together with the corresponding reciprocal-lattice diagram for the orientation used in these experiments is given in Fig. 3. The sample employed in these experiments was grown by Guggenheim of Bell Laboratories. The

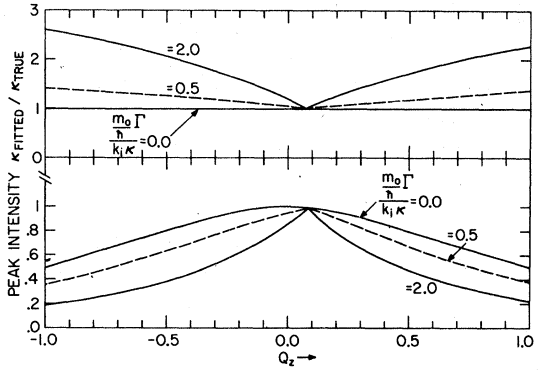

FIG. 2. Results of the computer simulation of a constant-angle experiment for various values of the reduced inelasticity $(m_0\Gamma/\hbar)/k_i\kappa$. Upper part of the figure gives the apparent κ divided by the true κ for various inelasticities as a function of Q_z. Lower part of the figure gives the peak intensity under the same conditions. Calculations were performed for $Q_z = 1$, $k_i = 6$, $\kappa = 0.05$.

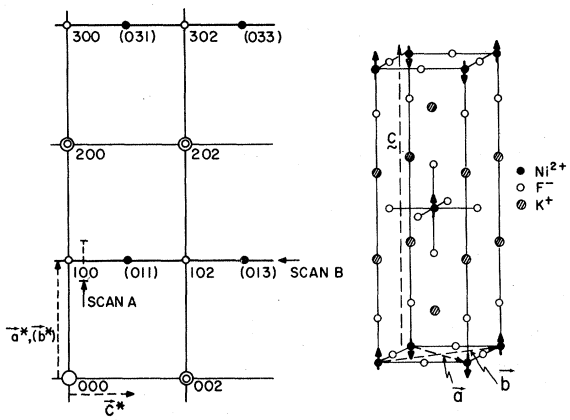

FIG. 3. Chemical and magnetic structure of K_2NiF_4. Inverting the central spin exchanges the a and b axes. Reciprocal lattice displays both the [010] and [100] magnetic zones. Nuclear Bragg peaks are indicated by double circles. Thick lines indicate the vicinity in which two-dimensional critical scattering is observed. Around $T_N = 97.23\,^\circ$K, $a^* = 1.112$ Å^{-1}, $c^* = 0.4818$ Å^{-1}.

sample and method of growth have been described previously.[2] The crystal is approximately 0.5 cm^3 in volume with a mosaic spread (full width at half-maximum) of 0.5 deg.

The elastic and inelastic experiments were carried out, respectively, on double- and triple-axis spectrometers at the Brookhaven High-Flux Beam Reactor. The elastic experiments were performed at wavelengths (λ) of 1.029 and 1.968 Å. The monochromator was a germanium crystal reflecting from (3, 1, 1) and (1, 1, 1), respectively, in transmission geometry. This choice of reflections minimized beam contamination from $\frac{1}{2}\lambda$ neutrons. 10-min horizontal collimation before the monochromator and both before and after the sample was employed (see Fig. 1). There was no explicit vertical collimation except for that determined by the collimator heights themselves. In these experiments this meant that one essentially integrated over the vertical coordinate of the scattering function. In the inelastic experiments, incoming energies varied between 5.2 and 56 meV depending on the energy range being studied and the resolution required. The monochromator and analyzer were both pyrolytic graphite reflecting from either (002) or (004). The collimators were also varied in order to optimize both the signal and the resolution wherever possible. The sample was mounted with its [010] magnetic axis vertical on an aluminum pedestal using Hysol Epoxy type 1 C; both the pedestal and glue were covered with cadmium. The sample holder was then mounted in a Cryogenics Associates temperature-control Dewar; around $T_N = 97.2\,^\circ$K relative temperatures were found to be reproducible to within 0.020 °K.

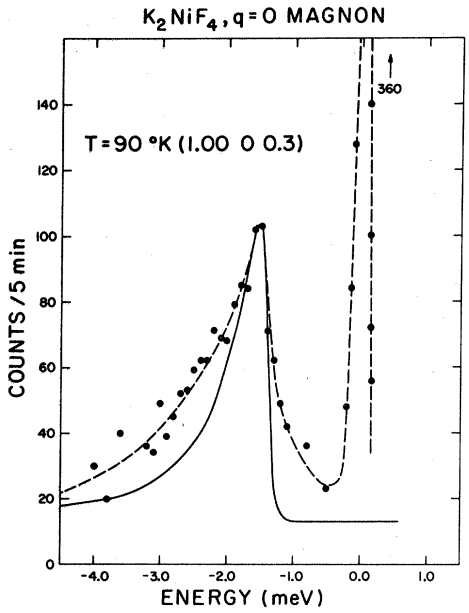

FIG. 4. Energy analysis of the scattering at $q=0$ for $T=90\,^{\circ}\mathrm{K}$, 7.2 °K below T_N. This experiment measures approximately $\mathcal{S}^{\parallel}_{D}(0,\omega)+\mathcal{S}^{\perp}_{D}(0,\omega)$. Solid line is the calculated line shape assuming perfectly sharp excitations. Dotted line is a guide to the eye.

B. Resolution Limitations

The ultimate precision of the experiment is limited by both the mosaic spread of the sample and the resolution limit of the instrument. In this case, the sample mosaic is rather large and hence could present a serious problem. Fortunately, however, since the critical scattering is [2], it is possible to avoid this difficulty. Consider the reciprocal-lattice diagram given in Fig. 3. At the (1, 0, 0) position the mosaic spread is perpendicular to the (1, 0, 0) vector and hence the mosaic in the plane is along the (1, 0, l) direction. However this is just the direction of the critical scattering ridge. Thus there is no first-order contribution of the sample mosaic to the ridge width around (1, 0, 0). There is, of course, a contribution to the vertical width. However, since our experimental arrangement is such that we effectively integrate over the vertical coordinate of the scattering function, the vertical mosaic has no effect.

The resolution function of a two-axis spectrometer can be described as an ellipsoid in reciprocal space where any cross section through the ellipse has a Gaussian intensity profile.[16] The resolution ellipse within the plane is illustrated in the bottom part of Fig. 1. To a first approximation it may be described as an elongated ellipse with the long axis nearly perpendicular to k_f. In our case it is only this long axis which is important.

The experimentally measured data are a convolution of the intrinsic cross section both with the mosaic function of the sample and with the instrumental resolution. As noted previously, for quasi-elastic experiments carried out around (1, 0, 0), the sample mosaic part of the convolution drops out. Over essentially the entire temperature range of interest to us here, the instrumental resolution is an important factor. The actual values for the parameters in $\chi(\vec{q})$ then must be deduced by least-squares fitting the chosen analytic form for $\chi(\vec{q})$ folded with the resolution function to the experimental data on a point-by-point basis. This procedure necessarily limits our ability to distinguish between the different analytic forms for $\chi(\vec{q})$. We shall discuss the actual implementation of the fitting procedure in Sec. V.

For the dynamic experiments, we must include in the resolution ellipse an additional variable – the energy. Since we do not carry out any explicit deconvolutions of our dynamic experiments, it is not worthwhile discussing this in any more detail here.

IV. EXPERIMENTAL RESULTS: DYNAMICS

As noted in the Introduction, previous studies of the dynamics in K_2NiF_4 have been limited to a measurement of the magnon dispersion relation at 4.2 °K and a brief survey of the thermal evolution of some long-wavelength magnons through T_N.[2] In this work, we consider first the behavior of $\mathcal{S}^{\parallel}(q,\omega)$ and $\mathcal{S}^{\perp}(q,\omega)$ at $q\simeq 0$ around T_N. Here $\mathcal{S}^{\parallel}$ is defined as the component of $\mathcal{S}^{\alpha\beta}$ along the spin direction (c axis) in the ordered phase; similarly, $\mathcal{S}^{\perp}$ is the component perpendicular to the c axis. Experiments around $q=0$ were carried out mainly with 5.2-meV incoming neutrons and with 40-min collimation before and after both the monochromator and analyzer. An energy scan at 90 °K at the position (1, 0, 0.3) is shown in Fig. 4. This scan measures approximately the combination $[\mathcal{S}^{\parallel}(\vec{Q},\omega)+\mathcal{S}^{\perp}(\vec{Q},\omega)]$. It should be emphasized that the magnetic Bragg peaks are [3] in character and therefore occur only at positions such as (1, 0, 0), (0, 1, 1), and (1, 0, 2) whereas the critical scattering is completely [2] in form; hence by going along the ridge away from the Bragg-peak position it is possible to observe the pure fluctuation spectrum without the complication of having to subtract off a Bragg peak as occurs in [3] critical scattering experiments. From Fig. 4 it may be seen that for $q=0$ at 90 °K the spectrum is composed of a sharp peak centered around $E=0$ and satellite peaks at ~1.5 meV (we show in Fig. 4 only the neutron energy gain peak). Measurements of the relative intensities of the peaks for various positions along the ridge, which in turn varies the relative contributions $\mathcal{S}^{\parallel}$ and $\mathcal{S}^{\perp}$, show that the central peak arises from $\mathcal{S}^{\parallel}$, the longitudinal fluctuations, whereas the peaks at ~1.5 meV arise from $\mathcal{S}^{\perp}$. The lat-

ter is, of course, just the spin-wave spectrum and 1.5 meV gives the spin-wave gap at 90 °K. The solid line in Fig. 4 is a calculation of the anticipated line shape arising from the spin waves assuming perfectly sharp excitations. The calculations were carried out using the convolution program of Samuelson and Hutchings[17] adapted for K_2NiF_4. The skew symmetry in the line shape is a resolution effect which arises from the fact that the magnon dispersion curves are quite steep so that the finite q resolution is important over a relatively wide range of energy. From the figure it may be seen that simple spin-wave theory gives a surprisingly good account of the line shape around $q=0$ even at 90 °K. The experimental spectrum is somewhat broader than the calculated one showing that there are some intrinsic lifetime effects but they are not appreciable.

The most surprising feature of the data at 90 °K is the longitudinal mode. This diffusive critical mode was not observed in the metallic ferromagnets iron[18] and nickel[19] below T_c and has only been previously observed in the insulating antiferromagnets MnF_2 and $RbMnF_3$.[8,9] The mode is found to be extremely sharp in energy. The measured width is 0.18 ± 0.03 meV compared with an instrumental resolution of 0.16 meV. Thus, to within the experimental error for $T_N - T = 7.2$ °K, there is no observable energy width in the longitudinal critical mode. This is in contrast with what might be expected from classical theory. Van Hove[20] first showed that for $T > T_c$ the spin fluctuations in a ferromagnet should speed up as one heats the sample above T_c. He suggested that this might also occur for $T < T_c$, but he did not treat this case explicitly because of the complications introduced by the presence of a permanent magnetization. This apparent elasticity of the critical fluctuations at $q=0$ for $T < T_c$ has also been inferred by Schulhof *et al.* for MnF_2.[9] They were not actually able to measure $\Gamma^{\parallel}(0)$ because of the presence of the magnetic Bragg peak but their finite q measurements of $\Gamma^{\parallel}(\vec{q})$ seemed to extrapolate to $\Gamma^{\parallel}(0)=0$. We anticipate our later results at this point to note that $S^{\parallel}(0,\omega)$ does indeed "speed up" for $T > T_c$. We are then faced with a very interesting dilemma: why is the speeding up observed for $T > T_c$ but not for $T < T_c$? It seems clear that the difference in behavior must be associated with the presence of the permanent sublattice magnetization for $T < T_c$. This problem has, in fact, been discussed in detail by Heller[21] in the context of MnF_2. He notes that the measured susceptibility χ_T may be factorized into two parts:

$$\chi_T = \chi_S + (T/C_H)(dM_0/dT)^2 . \qquad (15)$$

He postulates that for $T < T_c$ the first term χ_s has a very rapid relaxation rate (i.e., it *speeds up* below T_c), whereas the second term which is coupled to the energy, which is in turn a constant of the motion, must relax slowly near $q=0$. The explanation of our data thus would be that it is $(T/C_H) \times (dM_0/dT)^2$ which gives rise to the sharp peak in Fig. 4, whereas χ_s gives a broad distribution which would be lost in the background. From Fig. 4 it may be seen that at 90 °K we clearly cannot make any statement about the relative sizes of χ_T and χ_S.

The behavior of the transverse $q=0$ mode as a function of temperature through $T_N = 97.23$ °K is shown in Fig. 5. These measurements were carried out at the ridge position (1, 0, 2.3) which yields $\frac{1}{2} S^{\parallel}(0,\omega) + \frac{3}{2} S^{\perp}(0,\omega)$. A well-defined spin-wave gap is found to exist even at 97.0 °K, ~0.2 °K below the phase transition. The line shape is quite similar to that calculated at 90 °K (see Fig. 4) showing that simple spin-wave theory describes the long-wavelength magnons essentially right up to T_N. By 98 °K, ~0.8 °K above T_N, the gap has of course collapsed to zero. (This is not fully apparent

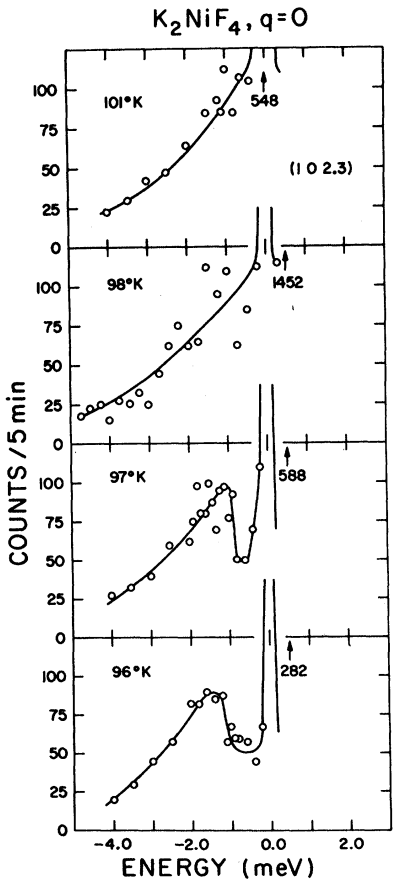

FIG. 5. Temperature variation through T_N of the transverse generalized susceptibility at $q=0$. Measurements were carried out at (1, 0, 2.3) which yields approximately $\frac{1}{2} S^{\parallel}_D(0,\omega) + \frac{3}{2} S^{\perp}_D(0,\omega)$. Solid lines are guides to the eye.

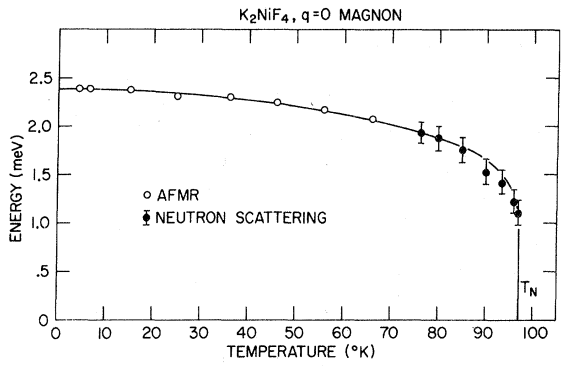

FIG. 6. Spin-wave gap energy vs temperature in K_2NiF_4. Solid line is the sublattice magnetization normalized to 2.37 meV at 4.2 °K.

from Fig. 5 because of the low statistics. However, longer runs carried out at other ridge positions illustrated the zero gap clearly.) It is important to note, however, that the transverse spectrum above T_N is quite similar to that below T_N, except for the collapse of the gap. There is no change in intensity through T_N nor is there any real change in the line shape. The longitudinal mode, on the other hand, diverges at T_N. The inelastic data then confirm in a very convincing fashion our previous observation based on the quasielastic data that only $\chi^{\parallel}(\vec{O})$, the component of the wave-vector–dependent susceptibility along the anisotropy axis, diverges at T_N. Figures 4 and 5 show clearly that $\chi^{\perp}(\vec{O})$ is nearly temperature independent over a wide range of temperature around T_N: hence, the conclusion that K_2NiF_4 exhibits an *anisotropy-induced* [2] *phase transition*.

Figure 6 shows the neutron measurements of the gap frequency as a function of temperature together with corresponding antiferromagnetic-resonance measurements by Birgeneau, DeRosa, and Guggenheim.[22] The solid line is the measured sublattice magnetization suitably scaled.[1,22] The two curves agree to within experimental error at all temperatures. We do not know of any fundamental theory which predicts such behavior but nevertheless our empirical observation of the simple relationship between the gap frequency and the sublattice magnetization is quite enticing.

We have also attempted to measure the q dependence of the inelasticity for $S^{\parallel}(q, \omega)$ at T_N. Here we expect the simple form $\Gamma^{\parallel}(\vec{q}) \propto q^z$, where the exponent z is to be determined by experiment. The measurements were carried out using 5.2-meV incoming neutrons with 20-min. collimation before and after both the monochromator and analyzer. It was found that reliable values of the energy widths could only be determined for wave vectors up to twice the q-resolution width (~0.005 Å^{-1} in this case). Over this entire range the observed energy widths were just those of the resolution function (0.10 meV). Thus the inelasticity at T_N over the q range for which we can make measurements is too small to be observable.

Several energy scans at $q = 0$ for $T > T_N$ are shown in Fig. 7. These were also carried out using 5.2-meV incoming neutrons but with 40-min horizontal collimation. As anticipated, the intensity decreases rapidly with increasing temperature and the energy width increases from 0.16 meV (~the resolution width) at 98 °K to ~0.25 meV at 105 °K. Thus we do indeed observe the anticipated slowing down of the longitudinal critical fluctuations as $T \to T_N^+$. Attempts to measure the q dependence of the relaxation rates for $T > T_N$ again were not successful. We therefore limit ourselves to the foregoing qualitative observations on the dynamics of the longitudinal critical fluctuations.

We now consider the temperature dependence of the spin waves away from $q = 0$. Previously, Skalyo *et al.*[2] observed that long-wavelength magnons ($q \sim 0.05$ Å^{-1}) exhibit little renormalization or lifetime effects right through T_N. We have now extended their measurements over the entire Brillouin zone. Typical experimental results for an intermediate-wavelength magnon, $q \sim 0.13$ reciprocal-lattice units (the zone boundary is at $q = 0.5$) and $E = 16$ meV, are shown in Fig. 8. These scans were carried out using the constant-E mode of operation, where the energy is held fixed while the momentum transfer Q is varied. The solid line accompanying

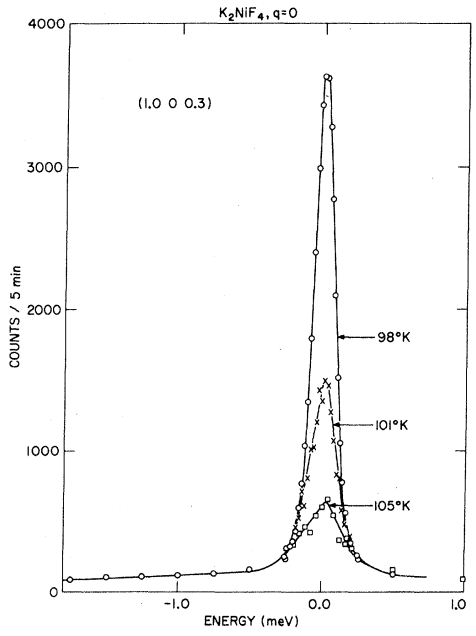

FIG. 7. Energy analysis of the longitudinal critical scattering at $q = 0$ for $T > T_N$. Long tail arises from the transverse fluctuations. Solid lines are guides to the eye.

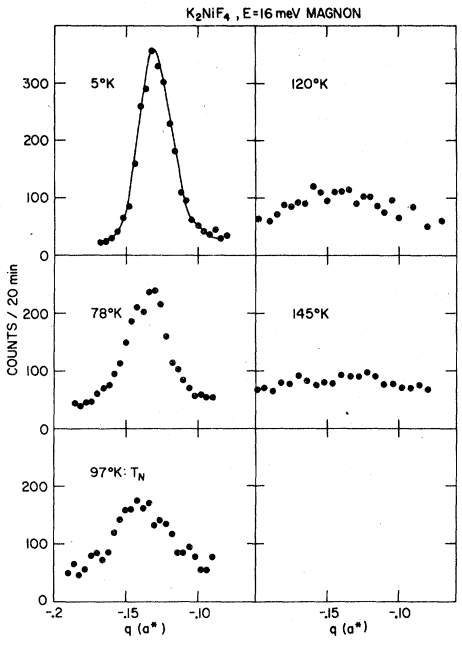

FIG. 8. Temperature dependence of the 16-meV magnon in K_2NiF_4. Solid line at 5 °K is the calculated line shape assuming perfectly sharp magnons.

the 5 °K data is the theoretical instrumental line shape calculated for magnons with infinite lifetimes. The parameters in the expressions for the magnon energies and structure factors have previously been determined by Skalyo *et al.*,[2] while the instrumental parameters are measured directly so that the only adjustable parameter is the over-all height. The agreement between this theory and experiment at 5 °K is excellent.

As the temperature is raised the peak height decreases while the line is broadened beyond the instrumental width, indicating that real lifetime effects are manifesting themselves. However, even at 97 °K magnons are still well-defined. The over-all intrinsic q half-width of the 16-meV magnon is about 0.015 ± 0.005 reciprocal-lattice units which corresponds to about 1.5 ± 0.5 meV in energy. The most interesting feature is that there has been little renormalization at all in the real part of the energy. As the temperature is raised further, up to 120 °K, the 16-meV magnon broadens considerably but still, nevertheless remains well-defined. We note from Fig. 8 that, to within the error, the center of the peak is not more than 10% away from that at 5 °K. Finally, by 145 °K the magnon has broadened sufficiently that with our present signal to noise we cannot make any statement about its nature. We have carried out similar measurements at 8, 12, 20, 24, 30, and 38 meV. In all cases the results are qualitatively the same as those at 16 meV, that is, there is at most a 10% decrease in the real part of the magnon energy up to the highest temperature measured whereas the imaginary part changes drastically. For the higher-energy magnons, signal to noise becomes a problem at an early stage since the intensity varies as $1/E$.

It is interesting to compare these measurements with corresponding measurements of the transverse susceptibility in the uniaxial [3] antiferromagnet MnF_2.[23,24] In that case, the magnon energies are renormalized by about a factor of 4 between 5 °K and $T_N = 67.46$ °K. In addition, the real and imaginary parts of the magnon energy are about equal at T_N so that the characterization of the transverse excitations as propagating modes is itself questionable. It seems likely that the difference in behavior between these [2] and [3] antiferromagnets resides in the difference of the ratios T_N/T_{ZB}, where T_{ZB} is the zone-boundary magnon temperature at 0 °K. In MnF_2 $T_N/T_{ZB} \simeq 1$, whereas in K_2NiF_4 this ratio is about 0.2. This means that in K_2NiF_4, even at T_N, only relatively long-wavelength magnons are thermally populated; simple spin-wave calculations[25] then indicate that under these conditions there should indeed be little renormalization of the real part of the energy. The surprising feature, however, is that as the temperature is raised above T_N, the destruction of long-range order and the subsequent continuous reduction in the longitudinal correlation length manifests itself only in the spin-wave lifetimes, not in their energy.

V. EXPERIMENTAL RESULTS: STATICS

The static experiments were carried out on a two-axis spectrometer with the configuration shown in Fig. 1 using neutrons of energy 77.2 and 21.1 meV. Before beginning a detailed study, it is necessary first to survey the gross qualitative features of $\chi^{\alpha\beta}(\vec{q})$. The most significant feature of the data has already been discussed in Ref. 3. There, measurements of $d\sigma/d\Omega$ at (1, 0, 0.2) and (1, 0, −6.8) at 105 °K using 77-meV incoming neutrons were reported. In the quasielastic approximation, the former measures $\chi^{\parallel} + \chi^{\perp}$ whereas the latter gives approximately $2\chi^{\perp}$. The result was that at (1, 0, −6.8) the scattering was weak and nearly independent of q. This led us to conclude that only $\chi^{\parallel}$ is diverging at T_N, a result which has been dramatically confirmed in the dynamic measurements reported in this paper. Because of the importance of $d\sigma^{\perp}/d\Omega$ in our data analysis it is worthwhile considering this matter in some more detail. Figure 9 gives similar measurements carried out at 100.96 °K with 21-meV incoming neutrons at (1, 0, 0.2), (1, 0, −5.8). These measure, respectively,

$$(1, 0, 0.2): f^2(\vec{Q}) \left(0.99 \frac{d\sigma^{\parallel}}{d\Omega} + 1.01 \frac{d\sigma^{\perp}}{d\Omega}\right)$$

and (16)

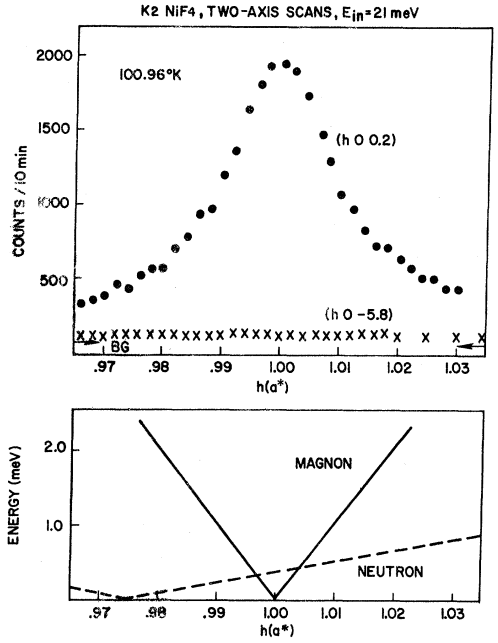

FIG. 9. Two-axis scans across the ridge at (1, 0, 0.2), (1, 0, −5.8) measured with 21-meV incoming neutrons. Bottom part of the figure gives the corresponding diagram in E-q space for the transverse part for a quasielastic measurement nominally at (0.975, 0, −5.8).

$$(1, 0, -5.8): f^2(\vec{Q})\left(0.14\frac{d\sigma^{\parallel}}{d\Omega}+1.86\frac{d\sigma^{\perp}}{d\Omega}\right).$$

At (1, 0, 0.2), k_f is very close to being parallel to the ridge so that the integration over the energy is carried out properly. Hence the measurement at (1, 0, 0.2) yields $\chi^{\parallel}+\chi^{\perp}$. At (1, 0, −5.8), however, k_f is nearly perpendicular to the ridge. The consequence of this for the transverse part is illustrated in the bottom portion of Fig. 9. To a first approximation, the E-q relationship for the transverse correlations around T_N is merely the magnon dispersion curve with slope 109 meV/Å^{-1}. There is, of course, some broadening but we can ignore this for our illustrative purposes here. The corresponding slope for the neutron-dispersion curve, however, is only 14.7 meV/Å^{-1}. Thus when the spectrometer is set to look at nominally elastic scattering at $h = 0.975$ one is in fact observing inelastic processes arising from h much closer to $h = 1.0$. This will be true for the entire range of h values covered in the scan shown in Fig. 9. Thus the fact that the scattering at (h, 0, −5.8) is flat tells us nothing about the corresponding variation of $\chi^{\perp}$. This was not properly appreciated in Ref. 3. From our point of view, however, the important feature of the scattering at (1, 0, −5.8) is that it is much weaker than that at (1, 0, 0.2). $d\sigma^{\perp}/d\Omega$ is probably also only weakly q dependent, but this has not been proven experimentally. To a good approximation, then, in our analysis of the quasielastic scattering at (1, 0, 0.2) the transverse component may be treated as part of the background. This will introduce some uncertainty but it should not be serious.

The second feature of $\chi^{\alpha\beta}(\vec{q})$ which we wish to examine is the validity of the quasielastic approximation for the longitudinal part for various geometries. Accordingly, scans along the top of the ridge at (1, 0, l) were carried out. Results of such a scan at 21 meV and 102.5 °K are shown in Fig. 10. The ridge intensity as a function of "l" is observed to deviate significantly from the anticipated $(1-\cos^2\theta_l)$ behavior. First, the ridge peaks at an $l \neq 0$ and second, the drop off in intensity appears much more rapid than $\cos^2\theta_l$. Comparison of Fig. 10 with the computer simulations given in Fig. 2 shows that this is indeed just the behavior predicted for a breakdown of the quasielastic approximation when

$$m_0\Gamma/\hbar k_i\kappa \sim 1 .$$

The arrow in Fig. 10 is the position at which $\sin\theta_f = 0$; that is, k_f is parallel to the ridge. The peak in Fig. 10 is not as sharp as that in Fig. 2 because of finite resolution effects in the former. We conclude, therefore, that as long as the measurements of $d\sigma^{\parallel}/d\Omega$ are carried out in the neighborhood of (1, 0, 0.4) at 21 meV, we will in fact measure $\chi^{\parallel}(\vec{q})$ properly. Similar results are obtained at 77 meV, although the effects of the breakdown of the quasielastic approximation are not so dramatic. In that case, $\sin\theta_f = 0$ at (1, 0, 0.2).

Typical scans across the ridge at 97.26 and 107.4 °K are shown in Figs. 11 and 12. In both cases the Lorentzian-like shape of $\chi^{\parallel}(\vec{q})$ is evident. The data above $h = 1.02$ were found to be contaminated slightly by a small satellite crystal and hence were omitted in the analysis. Scans similar to those shown in the figures were carried out at a series of temperatures between $T_N = 97.23$ and 110 °K with

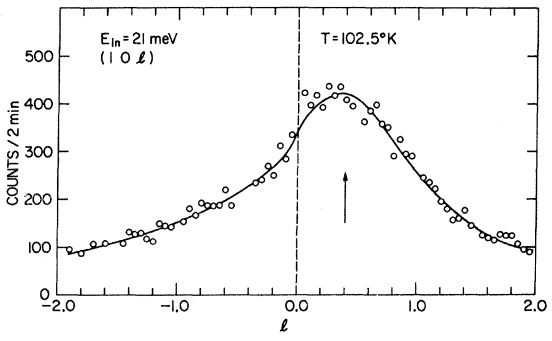

FIG. 10. Scan along the top of the ridge at (1, 0, l) in K_2NiF_4 with 21-meV incoming neutrons. This corresponds to scan B in Fig. 3. Arrow denotes the position at which k_f is perpendicular to the NiF_2 planes.

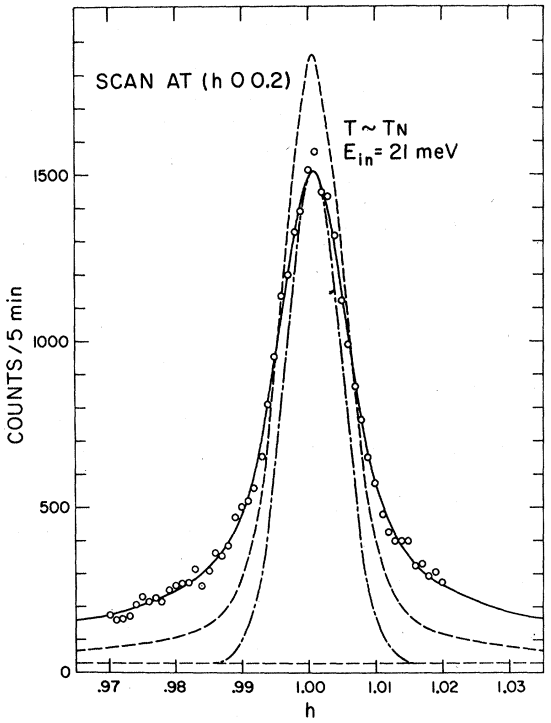

FIG. 11. Two-dimensional critical scattering in K_2NiF_4 at $T = 97.26$ °K. Center curve is the measured resolution function at (1, 0, 0). Solid line through the data points is a least-squares fit to $A/q^{2-\eta}$ with $\eta = 0.4$. Dotted line is a fit to the form $A/(\kappa^2+q^2)$ with κ fixed at 10^{-4} reciprocal-lattice units.

21-meV incoming neutrons and from T_N to 210 °K with 77-meV neutrons.

In order to deconvolute the data to obtain $\chi''(0)$, κ'', it is first necessary to decide on the proper analytic form for $\chi''(\vec{q})$. To begin with, we employ

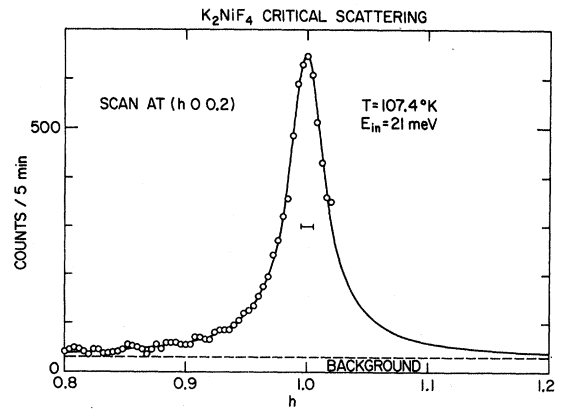

FIG. 12. Two-dimensional critical scattering in K_2NiF_4 at $T = 107.4$ °K measured with 21-meV incoming neutrons. Solid line is a least-squares fit to the form $A/(\kappa^2+q^2)$ with $\kappa = 0.0115$ reciprocal-lattice units. Small line in the center gives the resolution width.

the form used by previous workers, that is, Fisher and Burford's "first approximant," which is Eq. (8) with $\varphi, \psi = 1$. We then fit each of κ, η, an overall scaling factor A, and the background at each temperature. If this is indeed the correct analytic form for $\chi''(\vec{q})$, then we must find that η is temperature independent whereas A must be only weakly temperature dependent. The results of these fits for η at 21 meV are shown in Fig. 13. The effective η one finds using this "first approximant" is extremely temperature dependent. It decreases rapidly from 0.4 at T_N to ~0.1, at 3 degrees above T_N. For temperatures above 100 °K the uncertainty in η always includes 0, indicating that a simple Ornstein-Zernike form is adequate to describe the experimental data at these temperatures. This behavior is inconsistent with the choice $\varphi, \psi = 1$ but, in fact, is just what one expects from Fisher and Burford's second approximant [Eq. (8)] for φ very small, $\psi \simeq 1$. As we have noted previously, Eq. (8) predicts that very near T_N, that is, for $\kappa \ll \varphi q$,

$$\chi(\vec{q})/\chi_0 \sim (1/r_1)^{2-\eta}\,(\varphi^\eta/q^{2-\eta}) \quad , \tag{9}$$

whereas away from T_N and for $q < \kappa/\varphi$

$$\chi(\vec{q})/\chi_0 \sim (1/r_1^{2-\eta})(\kappa^\eta/\kappa^2+q^2) \quad . \tag{10}$$

Unfortunately, the experimental data do not permit the determination of a statistically meaningful φ at each temperature.

We consider first the data taken very near T_N with 21-meV incoming neutrons. It is found that

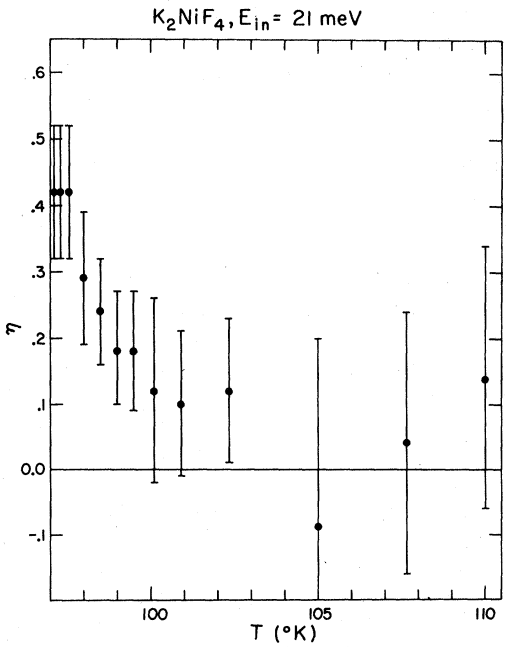

FIG. 13. Values of η deduced from the 21-meV data using Fisher and Burford's first approximant $[A/(\kappa^2+q^2)]^{1-\eta/2}$.

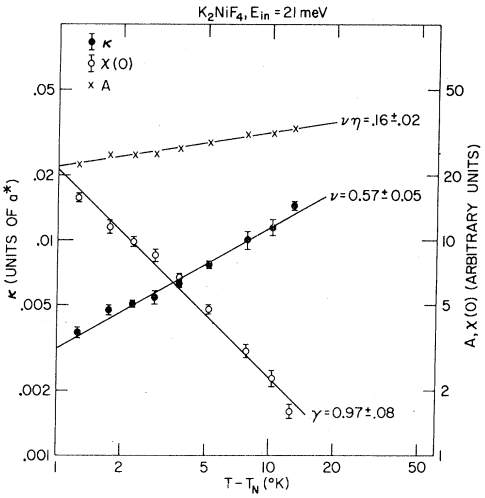

FIG. 14. Longitudinal inverse-correlation range $\kappa^{\parallel}$, staggered susceptibility $\chi^{\parallel}(0)$, and constant A in $\chi^{\parallel}(\vec{q}) = A/(\kappa^{\parallel 2} + q^2)$ determined at 21 meV. Solid lines are least-squares fits to power laws as described in the text.

$\chi^{\parallel}(\vec{q})$ reaches a limiting line shape at about 97.7 °K, 0.5 °K above T_N. The over-all intensity increases very slightly as T_N is approached but otherwise the successive curves for $\chi(\vec{q})$ are indistinguishable. Figure 11 shows the data taken at $T = 97.23$ °K. These are slightly above the $T_N = 97.23$ °K determined both from fits to the magnetization and from $\chi^{\parallel}(0)$; however they lie within the range covered by the spread in T_N indicated by the [3] magnetic Bragg scattering.[3] The inner curve in Fig. 11 is the measured resolution function. The solid curve is a least-squares fit to the data using Eq. (9). The fit gives

$$\eta = 0.4 \pm 0.1 \ . \tag{17}$$

The χ^2 goodness of fit is ~ 1, indicating that to within the accuracy of the data, Eq. (9) is a satisfactory analytic form. This value for η is found to be insensitive to the position chosen for the background.

In order to illustrate the difference between Eq. (9) with $\eta = 0.4$ and Eq. (10), we have also carried out a fit of the Ornstein-Zernike form to the data with κ fixed at the very small value of 10^{-4} reciprocal-lattice units to insure integrability at $q = 0$. This is shown as the dotted line in Fig. 11. From the figure it may be seen that the data differ significantly from the classical $1/q^2$ form.

We have fitted the data above T_N to the Ornstein-Zernike form

$$\frac{d\sigma^{\parallel}}{d\Omega} = \frac{AT}{\kappa^2 + q^2} \ , \tag{18}$$

where according to Eq. (10),

$$A \propto (1/r_1)^{2-\eta} \kappa^{\eta}, \quad \chi(0) = A/\kappa^2 \ . \tag{19}$$

For all temperatures above 99 °K the χ^2 is close to 1, again indicating that Eq. (18) is statistically adequate. A typical illustration of the quality of the fits is given in Fig. 12. The small line in the center gives the width of the resolution function. Even at 107.4 °K, 10 °K above T_N, the resolution function still contributes a significant portion of the total width.

From the least-squares fits to the data we obtain each of A, κ, $\chi^{\parallel}(0)$ as a function of temperature. These are plotted versus $T - T_N$ in Fig. 14. For a second-order phase transition, it is expected that in the asymptotic region both κ and $\chi^{\parallel}(0)$ will have simple power-law dependences on the reduced temperature with exponents ν and $-\gamma$, respectively.[26] Least-squares fits to the data obtained with 21-meV incoming neutrons give

$$\kappa = (0.042 \pm 0.07)((T/97.23) - 1)^{0.57 \pm 0.05}$$

and (20)

$$\chi^{\parallel}(0) = C((T/97.23) - 1)^{-0.97 \pm 0.08} \ ,$$

so that $\nu = 0.57 \pm 0.05$, $\gamma = 0.97 \pm 0.08$. The error bars correspond to two standard deviations. From Eq. (19) it is evident that the temperature dependence of A has contributions from both κ^{η} and $(1/r_1)^{2-\eta}$. If we make the *ad hoc* assumption that κ^{η} is the dominant term, then we may obtain the product $\nu\eta$ from A. We find

$$A \propto ((T/97.23) - 1)^{0.16 \pm 0.04} \ , \tag{21}$$

so that

$$\nu\eta^* = 0.16 \pm 0.04$$

or (22)

$$\eta^* = 0.3 \pm 0.1 \ .$$

There are two major sources of uncertainty in the above analysis. First, the resolution width is nearly always comparable with the intrinsic width so that we rely heavily on the accuracy of the convolution procedure. Second, there is some difficulty involved in our inclusion of $d\sigma^{\perp}/d\Omega$ in the background. These uncertainties may be largely removed by repeating the entire experiment with incoming neutrons of quite different energy so that the resolution function is significantly altered. Accordingly, we have measured $\chi^{\parallel}(\vec{q})$ between T_N and 210 °K using neutrons of energy 77 meV. This increases the resolution width by about a factor of 2. The general features of the data taken at 77 meV are identical to those obtained at 21 meV. We first fit the data near T_N using Eq. (9). This gives

$$\eta = 0.4 \pm 0.1 \ , \tag{23}$$

in precise agreement with the previous value. We then fit the data above T_N using the Ornstein-Zernike form for $\chi^{\parallel}(q)$. The data for $\chi^{\parallel}(0)$, κ obtained

from scans across the ridge at (1, 0, 0.1), are shown in Fig. 15. Least-squares fits to the data with $T - T_N \lesssim 15\,^\circ\mathrm{K}$ give

$$\kappa = (0.048 \pm 0.010)((T/97.23) - 1)^{0.57 \pm 0.07}$$

and (24)

$$\chi^{\parallel}(0) = C'((T/97.23) - 1)^{-1.03 \pm 0.08},$$

so that $\nu = 0.57 \pm 0.07$, $\gamma = 1.03 \pm 0.08$. The scatter in A is such that it is not possible to obtain a meaningful value for $\nu\eta^*$. The precise agreement between each of the exponents η, ν, γ obtained at 21 and 77 meV is most gratifying. We note that the absolute values obtained for κ_0, that is, 0.042 ± 0.07 and 0.048 ± 0.010 reciprocal-lattice units, also agree to well within the experimental errors.

Above about 115 °K, the susceptibility and correlation lengths are observed to depart from their asymptotic behavior. This is, of course, to be expected. We note that κ is still relatively small at 210 °K; the value of $\kappa = 0.2$ reciprocal-lattice units corresponds to a correlation length of about 6 Å.

Our quasielastic measurements thus yield the following critical exponents:

$$\eta = 0.4 \pm 0.1, \quad \nu = 0.57 \pm 0.05, \quad \gamma = 1.0 \pm 0.1\,. \quad (25)$$

With somewhat more theoretical uncertainty, from the data above T_N, we obtain

$$\eta^* = 0.3 \pm 0.1, \quad (26)$$

in agreement with the value obtained from the line shape near T_N. This agreement, of course, is simply a statement of the fact that the scaling relation

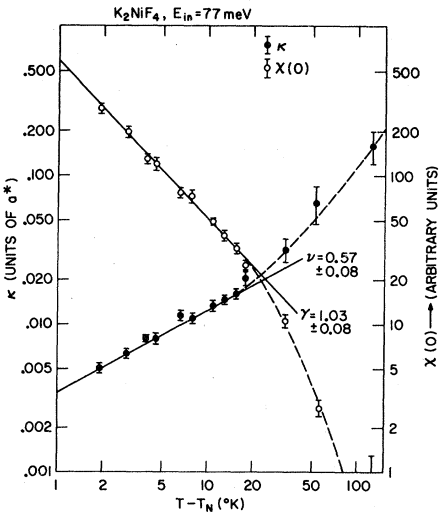

FIG. 15. Longitudinal inverse-correlation range $\kappa^{\parallel}$ and staggered susceptibility $\chi^{\parallel}(0)$ determined at 77 meV. Solid lines are least-squares fits to power laws as described in the text.

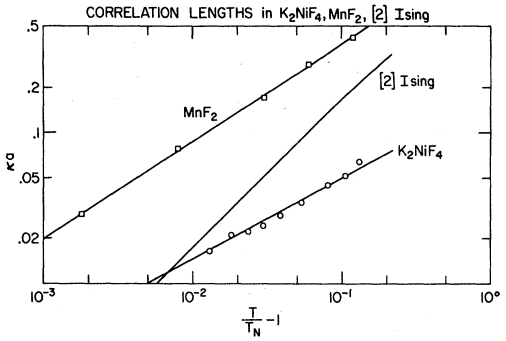

FIG. 16. Inverse-correlation ranges for K_2NiF_4, MnF_2, and the [2] $S = \frac{1}{2}$ Ising model. a is the separation between nearest-neighbor antiferromagnetic spins.

$$\nu(2 - \eta) = \gamma \quad (27)$$

is satisfied to within experimental error. We should note that our final values for the exponents ν, γ rest heavily on our assumption of a Lorentzian line shape away from T_N. Thus, for example, a fit of Fisher and Burford's "first approximant" with $\eta = 0.3$ to all of the data yields a ν nearer to 0.8. However, as we have noted previously, the data do seem to indicate that the Lorentzian form is to be preferred, albeit with rather low statistical confidence (see Fig. 13).

It is of interest to compare our values for the inverse longitudinal correlation lengths with those obtained experimentally for MnF_2[9] and with the exact result for the [2] Ising model.[13] These are shown in Fig. 16. The major difference between the [2] uniaxial antiferromagnet K_2NiF_4 and the [3] system MnF_2 seems to be in the magnitude of the correlation length rather than in the actual exponent although the latter does differ slightly in the two systems. At a given reduced temperature, say $T/T_N - 1 = 0.1$, the correlations are about 20 times larger in K_2NiF_4. Most surprisingly, however, there seems to be no correspondence at all between K_2NiF_4 and the [2] Ising predictions. This is true both for κ and for $\chi^{\parallel}(0)$. The [2] Ising model predicts exponents of 1, $\frac{7}{4}$, respectively, whereas we find 0.57, 1.0. The latter are, in fact, suggestively close to the molecular-field predictions of $\frac{1}{2}$, 1 although this is probably coincidental. Finally, we note that our value for $\eta = 0.4 \pm 0.1$ differs significantly from the classical value $\eta = 0$ but is rather close to the [2] Ising value of $\frac{1}{4}$.

In the Introduction to this paper, we noted that the numerical work of Jasnow and Wortis in three-dimensional systems indicates that the critical exponents should depend on the symmetry of the Hamiltonian alone and not on its details. On this basis we anticipated that we would observe critical behavior similar to that predicted for the [2] Ising

model. Our measurement of β, 0.138 ± 0.004, seemed to support this approach. It is clear, however, that our values for γ, ν are not consistent with this picture. It is difficult to offer a satisfactory explanation for this and indeed any convincing arguments probably will have to rest on detailed theoretical calculations. It is worthwhile, however, commenting on several possible pitfalls. The most obvious objection is that our measurements of γ, ν were not made in the asymptotic region. This can never be dealt with unambiguously in the absence of a detailed theory. However, we might note that over the entire region measured, only $\chi''(0)$ was appreciable; this is just what one expects in the Ising limit.[27] Second, one might speculate that the exponents are being affected by the [3] aspects of the system. This is also implausible. We should re-emphasize that the values for κ, $\chi''(0)$ are deduced from a [2] ridge, not a [3] peak. Furthermore, over the entire temperature range measured, and indeed right up to T_N, the critical fluctuations remain [2] in form with no suggestion of [3] correlations. If ν, γ were to be affected by the [3] interactions, then it would seem that as a prerequisite the three dimensionality of the system would have to manifest itself in the fluctuation spectrum. It does not.

These results clearly call for more research on both the experimental and theoretical levels. The differences in the temperature behavior of the transverse excitations in K_2NiF_4 compared with typical [3] systems such as MnF_2 are quite marked. A quantitative explanation of these differences presents a real challenge to the theorists. Similarly, numerical calculations of the static critical exponents in a [2] near-Heisenberg system would be valuable. On the experimental level, it is apparent that measurements of the critical exponents, in particular γ and ν, in similar [2] systems such as K_2MnF_4 would be most useful in order to test the universality of the behavior we observe in K_2NiF_4.

ACKNOWLEDGMENTS

We should like to acknowledge stimulating conversations on various aspects of this work with M. E. Fisher, P. Heller, P. C. Hohenberg, P. C. Martin, M. P. Schulhof, and R. Silberglitt. We should also like to thank P. C. Hohenberg for a number of helpful comments on the manuscript.

---

*Work performed under the auspices of the U.S. Atomic Energy Commission.

[1]R. J. Birgeneau, H. J. Guggenheim, and G. Shirane, Phys. Rev. Letters 22, 720 (1969); Phys. Rev. B 1, 2211 (1970).

[2]J. Skalyo, Jr., G. Shirane, R. J. Birgeneau, and H. J. Guggenhim, Phys. Rev. Letters 23, 1394 (1969).

[3]R. J. Birgeneau, J. Skalyo, Jr., and G. Shirane, J. Appl. Phys. 41, 1303 (1970).

[4]Support for this picture is given by recent experiments in the linear chain antiferromagnet $CsMnCl_3 \cdot 2H_2O$ [J. Skalyo, Jr., G. Shirane, S. A. Friedberg, and H. Kobayashi, Phys. Rev. B 2, 1310 (1970)]. In this case, the phase transition is driven by the [3] aspects of the system and indeed it is found that near T_c the critical scattering goes over to being [3] in form. This, of course, is not the case in K_2NiF_4.

[5]M. D. Mermin and H. Wagner, Phys. Rev. Letters 17, 1133 (1966). Note, however, that the absence of long-range order for $T > 0$ does not preclude a divergence of the susceptibility. See G. S. Rushbrooke and P. J. Wood, Mol. Phys. 1, 257, (1958); H. E. Stanley and T. R. Kaplan, Phys. Rev. Letters 17, 913 (1966).

[6]D. Jasnow and M. Wortis, Phys. Rev. 176, 739 (1969).

[7]R. A. Ferrell, N. Menyhard, H. Schmidt, F. Schwabl, and B. Szepfalusy, Phys. Rev. Letters 18, 891 (1967); B. I. Halperin and P. C. Hohenberg, Phys. Rev. 177, 952 (1969).

[8]H. Y. Lau, L. N. Corliss, A. Delapalme, J. M. Hastings, R. Nathans, and A. Tucciarone, Phys. Rev. Letters 23, 1225 (1969).

[9]M. P. Schulhof, P. Heller, R. Nathans, and A. Linz, Phys. Rev. Letters 24, 1184 (1970).

[10]W. Marshall and R. Lowde, Rept. Progr. Phys. 31, 705 (1968).

[11]H. B. Callen and T. A. Welton, Phys. Rev. 83, 34 (1951); R. Kubo, Rept. Prog. Phys. 29, 255 (1966).

[12]M. E. Fisher and R. J. Burford, Phys. Rev. 156, 587 (1967).

[13]B. Kaufman and L. Onsager, Phys. Rev. 76, 1244 (1949).

[14]L. P. Kadanoff, Nuovo Cimento 44, 276 (1966); T. T. Wu, Phys. Rev. 149, 380 (1966).

[15]P. Heller, Rept. Progr. Phys. 30, 806 (1967); M. P. Schulhof, P. Heller, R. Nathans, and A. Linz, Phys. Rev. B 1, 2304 (1970).

[16]M. J. Cooper and R. Nathans, Acta. Cryst. A24, 619 (1968).

[17]E. J. Samuelson and M. T. Hutchings (unpublished).

[18]M. F. Collins, V. J. Minkiewicz, R. Nathans, L. Passell, and G. Shirane, Phys. Rev. 179, 417 (1969).

[19]V. J. Minkiewicz, M. F. Collins, R. Nathans, and G. Shirane, Phys. Rev. 182, 164 (1969).

[20]L. Van Hove, Phys. Rev. 95, 1374 (1954).

[21]P. Heller (to be published).

[22]R. J. Birgeneau, F. De Rosa, and H. J. Guggenheim, Solid State Commun. 8, 13 (1970).

[23]A. Okazaki, K. C. Turberfield, and R. W. H. Stevenson, Phys. Letters 8, 9 (1964).

[24]M. P. Schulhof, P. Heller, R. Nathans, and A. Linz (to be published).

[25]R. Silberglitt (private communication). See also the work on $CrBr_3$ by E. J. Samuelson, R. Silberglitt, G. Shirane, and J. P. Remeika (unpublished). In this system, which approximates a planar ferromagnet, the spin-wave energy is nearly constant up to T_c but by T_c the spin waves have broadened so severely that they can no longer be observed.

[26]M. E. Fisher, Rept. Progr. Phys. 30, 615 (1967).

[27]The fact that we might not be in the asymptotic regime would also manifest itself in higher-order terms in the expression for κ, that is, we could have

$$\kappa = \kappa_0 \tau^{\nu}(1 + a\tau + b\tau^2 \cdots) \ .$$

If a and b were much greater than unity, then our values for ν obtained from a simple power law ($a, b = 0$) could be grossly in error. With our present data we certainly cannot distinguish between various analytic forms for κ; hence we must simply assume a simple power law for the reduced temperature dependence until a detailed theory dictates otherwise. It is perhaps worth commenting, however, that the pertinent parameter may well be κ itself rather than τ and in that case, it is more likely that we are in the asymptotic regime.

PHYSICAL REVIEW B VOLUME 3, NUMBER 5 1 MARCH 1971

New Approach to Green's-Function Decoupling in Magnetism with Specific Application to Two-Dimensional Systems

M. E. Lines
Bell Telephone Laboratories, Murray Hill, New Jersey 07974
(Received 18 May 1970)

Existing first-order Green's-function theories of the Heisenberg ferromagnet all lead to magnon energies for which the temperature renormalization is wave vector independent. Such theories can describe phase transitions only at a temperature T_C for which *all* spin-wave excitations have vanishingly small energy. It has become increasingly evident, particularly for systems of low dimensionality, that such an approximation is quite unphysical, paramagnetic magnons often being physically well defined over much of the Brillouin zone to quite elevated temperatures. This paper describes a rather general method for introducing wave-vector-dependent magnon renormalization into the Green's-function formalism, enabling approximations of obvious physical significance to be made directly in terms of the magnon dispersion relation. The theory is developed in detail for the simplest nontrivial approximation and applied to the problem of the two-dimensional Heisenberg ferromagnet. A phase transition is found to a state of zero magnetization and infinite susceptibility. We also discuss the weakly anisotropic two-dimensional ferromagnet, which supports long-range order at low temperatures, and study the approach to the isotropic limit.

I. INTRODUCTION

Over the past several years, the technique of double-time temperature-dependent Green's functions has been applied with some success by many authors to a varied selection of statistical problems in ferro-, ferri-, and antiferromagnetism. Formally, the method produces solutions for the desired expectation values as functions of temperature, but these solutions are in the form of an infinite set of coupled first-order differential equations, and the development of a tractable formalism makes necessary a decoupling approximation.

The majority of decoupling procedures devised for Heisenberg systems, particularly in approximations applicable for general spin quantum number and aiming for validity over the entire temperature range, are made at the earliest possible stage of the calculation (i.e., in the differential equation involving the lowest-order Green's functions). This is done almost from necessity rather than choice, because of the enormous increase in mathematical complexity which results from delaying the decoupling to a later stage, [1] unless further approximations restricting the temperature range of validity are also introduced. A short list of publications, sufficient to give an indication of the developing sophistication in first-order Green's-function decoupling schemes, is given in Refs. 2–10.

Regardless of their degree of sophistication, these approximations all produce excitation energies for which the scaling with temperature is *wave vector independent*. That is, they all predict that short-wavelength and long-wavelength spin waves renormalize in the same way. A corollary is that they can describe well-behaved phase transitions only at the temperature for which *all* spin-wave-like excitations have vanishingly small energy. However, it is now well established experimentally that real magnetic second-order phase transitions are not at all like this but that the phase transition affects significantly only long-wavelength excitations. Both neutron diffraction[11,12] and Raman[13,14] experiments on magnetic systems reveal that short-wavelength excitations undergo no obvious anomaly at a phase transition temperature T_c but continue to exist well into the paramagnetic phase as propagating excitations. The phenomenon is most marked in systems of low dimensionality,[15,16] where all but the very long-wavelength spin waves are essentially temperature independent up to tem-